# Vibrating Reed Internal Friction Apparatus for Films and Foils

Abstract: An apparatus is described which permits for the first time the resolution of anelastic relaxation effects in evaporated metallic thin films and ion-implanted surface layers of silicon. The composite samples consist of the film or layer of interest on a carrier substrate having the form of a thin cantilevered reed. Low external losses and an exceptionally good span of operating frequencies are obtained by integrally bonding the substrate to a supporting pedestal and by using electrostatic drive and detection for the transverse modes of vibration. The internal friction can be measured with relatively simply instrumentation, at pressures below  $10^{-5}$  torr  $(1.33 \times 10^{-3} \text{ Pa})$  and over the temperature range  $-190^{\circ}\text{C}$  to  $550^{\circ}\text{C}$ . The apparatus has considerable versatility for work in a number of areas, including the investigation of metallic foils prepared by splat-cooling.

#### Introduction

The study of anelastic relaxation processes has been of considerable value in materials research, principally because of the insight provided into the nature and behavior of crystal defects at an atomic level [1]. The best known and most sensitive method for the detection of anelastic behavior is the measurement of internal friction as a function of temperature and/or vibration frequency. Of the various types of apparatus designed for this purpose, those utilizing a resonance method (as exemplified by either the torsion pendulum or resonant-bar apparatus) have been the most widely used [2]. Despite many individual differences, virtually all internal friction apparatus has so far been designed for use with bulk materials. Over the last few years, however, several areas of interest have emerged in which the available samples are extremely thin. For these a vibrating reed apparatus appears to be the most attractive prospect for relaxation studies. These newer areas include the study of (a) splatformed foils, (b) thin films, and (c) ion-implanted layers. For category (a), a suitable reed specimen can be cut directly from the foils produced by a number of liquidquenching methods, such as the piston-and-anvil or the rotating-roller methods [3, 4]. The reed is comprised entirely of the material under investigation, as is the case for bulk materials. For category (b), however, an evaporated or sputtered film is usually too thin to be made into a self-supporting reed, even if removal from the substrate were desirable and presented no difficulty. Consequently, the approach adopted here has been to use a composite sample consisting of the thin film deposited on a suitably chosen thin reed substrate of low internal friction. This approach, discussed briefly and somewhat

pessimistically by Benoit [5], had been pursued earlier with limited success by Weiss and Smith [6]. Based on present findings, however, it represents an attractive alternative or supplement to the use of self-supporting thick films, a direction taken by Postnikov and his coworkers [7].

The factors involved in the study of ion-implanted layers [item (c)] are very similar to those for thin films since the thicknesses are about the same in both cases (roughly 0.1 to 1  $\mu$ m). Following implantation, a reed of a convenient practical thickness (50  $\mu$ m) effectively becomes a composite sample consisting largely of unimplanted material, which acts as a carrier substrate for thin implanted near-surface layers. In studies of the surface film or layer, it is necessary that the losses within the carrier substrate do not mask the losses of interest. Since the substrate may typically be two orders of magnitude thicker than the surface layer, the substrate must be of comparatively low internal friction. This matter is discussed quantitatively later in the paper; it suffices here simply to state that an excellent resolution of effects has been obtained in the case of metallic thin films on fused silica substrates, and in ion-implantation studies of single crystal reeds of silicon [8].

#### Design features of the apparatus

## • Pedestal mounting of reed samples

The apparatus is suitable for use with reed samples 2 to 4 cm long, 0.3 cm wide and 0.005 cm thick. Samples of considerably greater thickness can be accommodated, but generally the objective has been to use a reed of

minimal thickness. When supported at one end as a cantilever reeds of these dimensions possess a fundamental flexural frequency of typically 40 to 100 Hz. Depending on the particular dimensions and damping levels encountered, it is usually possible to make internal friction measurements at the fundamental frequency and at a substantial number of overtones (see the section on frequency-related phenomena). The use of the first four tones, giving a frequency variation of a factor of over 30, is common practice; for long reeds of low internal friction, measurements have been made up to the eleventh tone, a frequency 300 times that of the fundamental.

For reeds of low internal friction, the method of mounting the reed is of major importance in securing a low external loss. Good results have been obtained by making an integral bond to an intermediate supporting pedestal which can be secured in turn to a supporting assembly (Fig. 1) by simple clamping springs. For studies of thin films, we have used 2-mil (50-\mu m) reeds of substratequality fused silica from the Dell Optics Corporation. The logarithmic decrement exhibited by such a pedestalmounted reed is about 10<sup>-5</sup>. Similar low damping levels have also been obtained from thin reeds of single crystal silicon, joined to silicon bases by a fine fillet of pure germanium. For metallic reeds, such as those produced by splat-cooling, the internal friction is usually high enough that a simple mechanical clamp is a satisfactory method of support.

Apart from the chief consideration of providing a low-loss support, the use of a pedestal mounting has other useful features. The pedestal and reed form a permanent unit that can be removed from and returned to the apparatus without changing the damping or frequencies exhibited by the sample. Consequently, it is possible to detect reliably even small changes resulting from treatments that are most conveniently administered outside the internal friction apparatus. These treatments include, for example, thin film deposition, ion implantation (or other types of irradiation), and annealing at temperatures beyond the range of the internal friction apparatus itself, i.e., > 500°C.

#### ◆ Mechanical layout

Figure 1 shows the specimen holder and electrode assembly designed for use with the pedestal-mounted reeds. The reed (1) is mounted in a frame consisting of two rectangular end-plates (2) held together by four tie rods (3), shown partly cut away for clarity. The pedestal base fits in a central recessed groove in one of the end-plates, and is firmly held in position (and electrically grounded) by two tungsten U-springs. The spring pressure can be controlled by the position of the sliding tension plates (5) and may be released by loosening the screws (4). Each electrode (6) is mounted on an insulating support tube

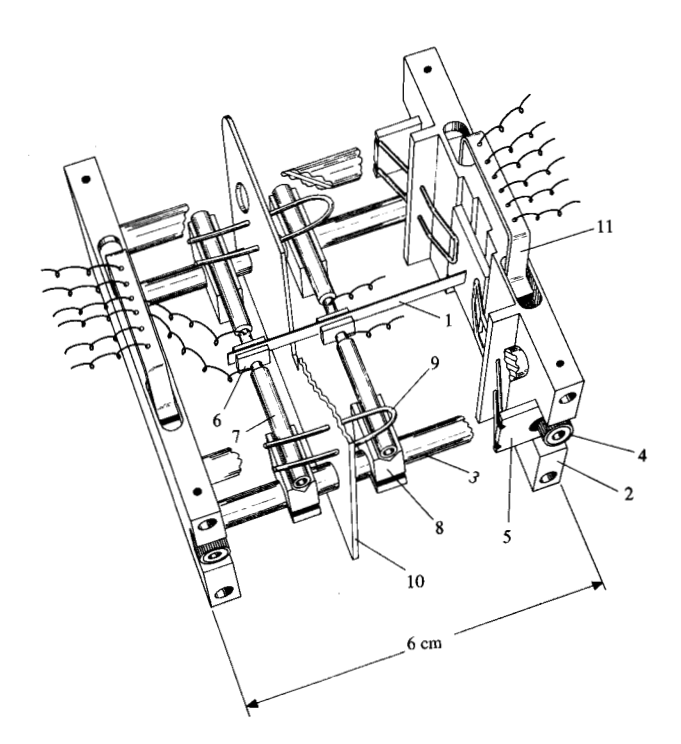


Figure 1 The sample holder, 1: pedestal-mounted reed; 2: end-plate; 3: tie-rod (shown partly cut away); 4: spring release screw; 5: tension plate; 6: electrode; 7: insulating electrode support tube; 8: V-block electrode supports; 9: spring clip; 10: slotted screening plate (shown partly cut away); 11: terminal strip.

(7), which may be of fused silica. High-purity alumina tubes, however, have better insulation resistance at high temperatures. The electrodes are secured in place by the spring action obtained by slitting the electrode shank where it is inserted into the tubes (7). These tubes are mounted in V-blocks (8), clamped to the tie-rods (3), and are held in place by the U-springs (9), suitably tensioned by their position in holes in the plate (10), shown partly cut away for clarity. The chief function of the plate is to screen the detection electrodes from the ac voltage applied to the drive electrodes. The screen is slotted vertically from the top edge to avoid interference with the assembly of the specimen; for minimal pickup this slot is subsequently closed by other auxiliary plates. A narrow clearance gap, however, remains around the reed. The U-spring pressure holds the tubes (7) securely but permits them to be pushed along the V-blocks for adjustment of the electrode gap distances.

Typical clearances between the electrodes and the faces of the reed are 0.076 cm (0.030 in.) for the drive electrodes (located at the free end of the sample) and 0.051 cm (0.020 in.) for the detection electrodes located closer to the fixed end of the reed. The position of the detection electrodes is chosen so as to avoid a nodal position for any of the tones of interest (see the Appen-

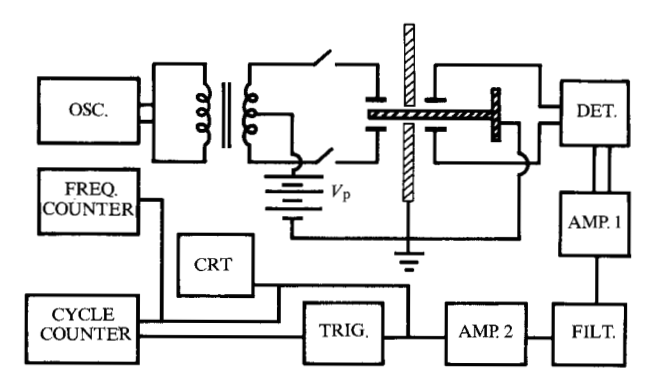


Figure 2 Block diagram of the drive and detection circuits.

dix). Usually, a position about one-third of the length of the sample from the fixed end serves well. The two standoff terminal strips (11) are made of silica.

The assembly of Fig. 1 is mounted inside a heater enclosure comprising two interlocking U-sections. This enclosure and the main parts of the specimen holder are made of nickel-plated copper. The heater enclosure is supported inside a vacuum chamber by stainless-steel tubes which pass through a demountable vacuum flange and terminate in various standard electrical feed-throughs. The vacuum chamber may be cooled with liquid nitrogen to provide an overall operating range of -190°C to 550°C. For protection against external vibrations the apparatus may be either suspended from a cushioned ceiling support or bolted to a concrete slab resting on rubber mountings.

#### • Electronic circuitry

A block diagram of the system of push-pull electrostatic drive and capacitor microphone detection is given in Fig. 2. The items shown are commercially available with the exception of three units, which can be built without difficulty. A Muirhead D-890-B decade oscillator (OSC in Fig. 2) serves as an ideal source of the ac drive voltage. The oscillator output is fed to a high-impedance audio transformer whose center-tapped secondary is connected to the polarizing batteries  $V_{\rm p}$ . The transformer output is fed to the drive electrodes via off-on switches and 100-k $\Omega$ current-limiting resistors. The magnitude of the fundamental component of the dynamic force exerted on the reed with this excitation arrangement is readily shown to be proportional to the product of  $V_n$  and the ac voltage,  $v_1 \sin \omega t$ . To minimize pickup it is advantageous to work with large values of  $V_{\rm p}$  and small values of  $v_{\rm i}$ . For most purposes, a single 90-V battery is more than sufficient for the polarizing voltage; however, a selector switch capable of furnishing two to three times this voltage can be useful for measurements at high frequencies and/or high levels of internal friction.

The push-pull transducer detection circuit (DET, Fig. 2) is a simple but highly sensitive one-tube design developed and analyzed in this laboratory by Tomboulian [9].

The output of this unit is amplified and converted to a single-ended signal by the laboratory-built unit AMP 1, which provides an adjustable voltage gain of up to 100. The signal is next filtered of extraneous noise (FILT in Fig. 2 is a Krohn-Hite Model 3550R variable bandpass filter) and further amplified by AMP 2 (Hewlett-Packard Model 465A). The resulting signal is visually monitored for absence of noise and distortion with the oscilloscope CRT and is fed to both an electronic counter (Hewlett-Packard Model 5245L) and a modified version of the trigger circuit described by Smith [10] for determination of the logarithmic decrement. Briefly, the function of this circuit is to emit two pulses which start and stop the operation of the cycle counter. The start pulse is produced when the voltage signal corresponding to the free decay of the sample vibration falls to a selected voltage level V<sub>1</sub>, and the stop pulse follows when the voltage has further decayed to a level  $V_2$ , generally chosen to be approximately half of  $V_1$ . The logarithmic decrement is obtained from the relation

$$\delta = (1/n) \ln \left( V_1 / V_2 \right), \tag{1}$$

where n is the number displayed by the cycle counter. This arrangement has provided highly reproducible and consistent results over a wide frequency range. Occasional use has also been made of alternative measurement schemes, such as the determination of  $Q^{-1}$  from the bandwidth of the resonance curve in forced vibration [11].

#### Operational characteristics of the apparatus

## • External energy losses

In the design of internal friction apparatus, careful attention must be given to external energy losses, which tend to mask the intrinsic behavior of the sample. Three sources of external loss in the present apparatus are considered here: air damping, transducer losses, and support losses.

## Air damping

At normal pressures the damping imposed on a thin reed by the surrounding atmosphere can be much larger than the internal friction of the sample itself. This phenomenon has been known for many years and, indeed, has found limited practical use in various vibrating-reed pressure gauges [12-14]. Data on air damping for thin reed samples used here are shown in Fig. 3 (a). It is evident that at normal atmospheric pressure, the air damping can exceed the internal friction of the reed by a factor of over

1000. The pressure at which the loss becomes negligibly small varies appreciably from tone to tone and falls below  $10^{-5}$  torr  $(1.33 \times 10^{-3} \text{ Pa})$  for the fundamental mode. Reeds of higher internal friction than that of Fig. 3(a) are, of course, more tolerant of higher pressures. In general, however, adequate reduction of the atmospheric loss requires evacuation by a diffusion pump. Figure 3(a) also shows that at pressures below 0.1 torr the atmospheric damping contribution is simply proportional to the pressure P, although the magnitude of the proportionality factor varies according to the tone used. Above roughly 0.1 torr the pressure dependence becomes much less marked. This behavior can be understood in terms of a transition from molecular flow to viscous flow [15]. In the latter regime, the viscosity of a gas becomes independent of its pressure. For the low-pressure (molecular flow) region, we have calculated the logarithmic decrement produced by the air damping,  $\delta_A$ , using simple kinetic theory. The result is

$$\delta_{A} = 2P/f_{n}\rho d\bar{u},\tag{2}$$

where P is the air pressure,  $\bar{u}$  is the average molecular velocity  $(4.7 \times 10^4 \text{ cm/s} \text{ at room temperature})$ ,  $\rho$  and d are the density and thickness of the reed, and  $f_n$  is the frequency of the particular mode considered. As shown by the three broken curves in Fig. 3(a), the agreement of Eq. (2) with experiment is good in the low-pressure region.

A final noteworthy result, shown in Fig. 3(b), is the downturn evident in the resonant frequencies as the pressure approaches the normal atmospheric value. This loading effect is relatively small, amounting to a decrease of between one and two percent for the different tones. Nevertheless, the existence of such an effect should be recognized, since a two percent error in the determination of resonant frequency leads to a four percent error in the determination of the elastic modulus of the sample.

## Transducer losses

An assessment of the loss associated with the transducer system can be made by considering a series circuit consisting of a capacitor C, a resistance R, and a battery  $V_{\rm b}$ . The total capacitance C represents the sum of two terms,  $C_{\rm e}$  and  $C_{\rm s}$ , where  $C_{\rm e}$  is the capacitance formed between a fixed electrode and the grounded reed, and  $C_{\rm s}$  represents the remaining stray capacitance of the wiring. The transducer loss is found by calculating the work done by the vibrating reed per cycle of vibration in generating an ac voltage signal of amplitude  $v_{\rm o}$  across the resistance R. The loss, denoted by  $\Delta W_{\rm T}$ , and the voltage  $v_{\rm o}$  are given by

$$\Delta W_{\rm T} = \left(\frac{\pi (C_{\rm e} V_{\rm b} a_{\rm o})^2}{C_{\rm e}^2}\right) \frac{\omega CR}{1 + (\omega CR)^2}$$
(3)

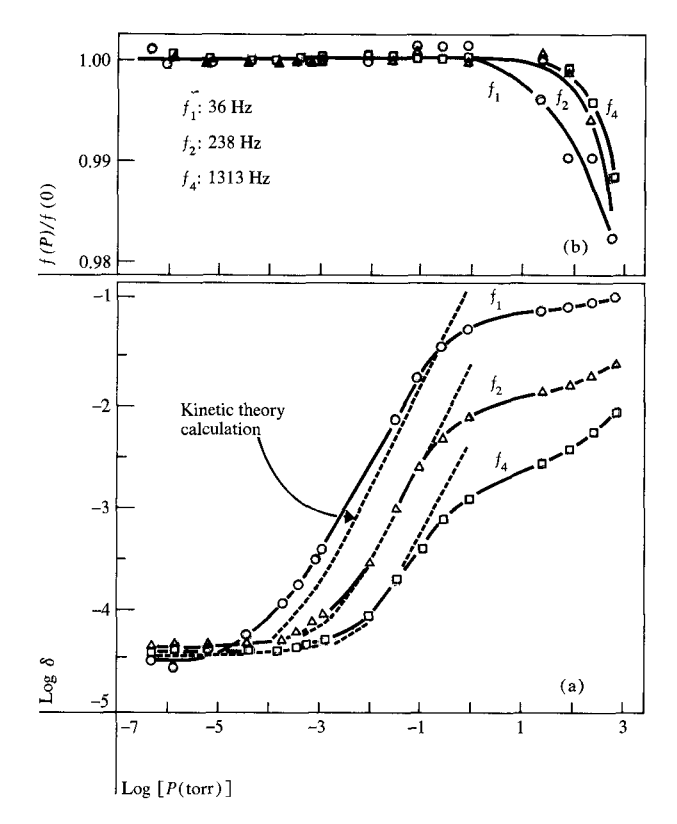


Figure 3 (a) Damping of a thin reed as a function of air pressure. (b) Resonant frequencies of the reed. The measurements were made at room temperature using the first, second, and fourth tones of vibration. The broken curves give the calculated air damping superimposed on the background internal friction of the sample. Note that the quantity plotted on the ordinate is the base-10 logarithm of the logarithmic decrement. The sample is a 50- $\mu$ m reed of fused silica with a 0.45- $\mu$ m film of niobium on each face.

and

$$v_0 = V_b \left(\frac{a_0 C_e}{gC}\right) \frac{\omega CR}{(1 + (\omega CR)^2)^{\frac{1}{2}}},$$
 (4)

where  $\omega$  is the circular frequency of vibration,  $a_0$  is the amplitude of motion of the reed at the position of the electrode, and g is the gap distance between the reed and the electrode. Equations (3) and (4) are derived with the condition, easily satisfied in practice, that  $(a_0C_e/gC)$  be small compared with one. Inspection of Eq. (4) shows that the detection sensitivity falls off when  $\omega\tau < 1$  (where  $\tau$  is written for the time constant CR) and tends to a limiting asymptotic value for  $\omega\tau > 1$ . On the other hand, it is seen from Eq. (3) that the loss  $\Delta W_T$  follows the classical Debye form, exhibiting a maximum at  $\omega\tau = 1$  and approaching zero asymptotically for both the high and low frequency limits. The optimal combination of high sensitivity and low loss is achieved in the region  $\omega\tau \gg 1$ .

337

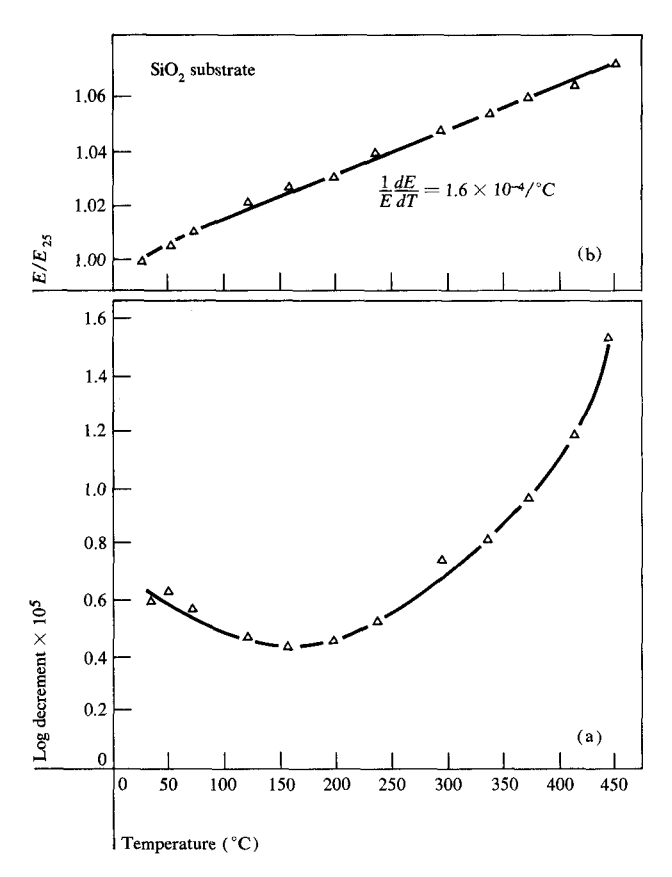


Figure 4 (a) Damping of a pedestal-mounted reed of fused silica, 50- $\mu$ m thick, of the type used as a substrate for thin-film samples; measurements in the fundamental mode at approximately 40 Hz. (b) The temperature dependence of Young's modulus E, relative to the value at 25°C, as deduced from the temperature dependence of the resonant frequency. Note the unusual positive sign of temperature coefficient (1/E)(dE/dT).

The logarithmic decrement  $\delta_T$  associated with the transducer loss is given by

$$\delta_{\mathrm{T}} = \Delta W_{\mathrm{T}} / K_{\mathrm{R}} A_{\mathrm{o}}^{2}, \tag{5}$$

where  $A_0$  is the amplitude of motion at the free end of the reed and  $K_n$  is the effective spring constant of the mode (as in the Appendix). After Eq. (3) is inserted into (5) it is seen that  $\delta_T$  is independent of amplitude (since  $a_0$  is proportional to  $A_0$ ) and depends on the square of the voltage  $V_b$ . Consequently, a convenient check on the absence of a significant detection loss can be made by repeating the damping measurement after a suitable change (say from 180 V to 90 V) in the supply voltage to the detection circuit. As an alternative procedure, the damping can be measured before and after one of the two electrodes has been disconnected and grounded.

## Support losses

The supported end of a cantilevered reed is the position of maximum surface strain for all tones of vibration.

Some energy loss to the support is therefore inevitable. Unlike the air and transducer losses discussed above, an independent assessment of this loss does not appear to be possible. However, the ability to measure logarithmic decrements below 10<sup>-5</sup> is an adequate indication that the support loss can be reduced to a very low level. By far the most important factor in the reduction of the loss is the elimination of mechanical slippage and rubbing friction at the root of the reed. Some procedures for making satisfactory integral bonds to a supporting pedestal have been mentioned earlier. An alternative procedure, described by Scott and MacCrone [16], is to form a reed and integral mounting support in one piece by cutting slits in a rectangular blank. This may prove a useful alternative to the pedestal mounting system for some applications.

The importance of a low-loss support is illustrated by the following remarks. With a pedestal mounting, the measured damping of a 50- $\mu$ m fused silica reed (Fig. 4) is fully two orders of magnitude smaller than that reported by Weiss and Smith [6] for ultrathin (about  $1\mu$ m) substrate reeds supported by a mechanical clamp. In terms of the sensitivity to film losses, the greater thickness of the present reeds is therefore more than compensated for by the reduction achieved in the level of damping. At the same time, the larger reeds used here provide much greater experimental convenience and the ability to work with many tones beyond the fundamental.

### • Transverse thermal current losses

Reeds in transverse vibration are subject to a calculable internal loss from a thermoelastic mechanism [17]. This loss is usually of no direct interest and simply contributes to the background damping. The magnitude of the loss can be calculated from the expression

$$\delta_{t} = (\pi E \alpha^{2} T / \rho S) f f_{0} / [1 + (f f_{0})^{2}],$$
 (6)

where E is Young's modulus,  $\alpha$  is the linear expansion coefficient, T is the absolute temperature,  $\rho$  is the density, S is the specific heat, and f is the vibration frequency of the reed. The frequency of peak loss,  $f_0$ , is given by

$$f_0 = \pi D_{\rm th} / 2d^2, \tag{7}$$

where  $D_{\rm th}$  is the thermal diffusivity and d is the reed thickness. The loss is small in fused silica because of the low expansion behavior of this material. The loss is also small in silicon below room temperature but can become appreciable at higher temperatures, particularly for frequencies approaching the peak frequency  $f_0$ .

## • Frequency-related phenomena

We consider now the frequency behavior of the reed, and factors that influence the determination of the elastic modulus. The frequencies  $f_n$  of the cantilever modes of a reed may be written in the alternative forms

$$f_n = \frac{2\alpha_n^2}{\pi l^2} \sqrt{\frac{EI}{\mu}} = \frac{\alpha_n^2 d}{\pi \sqrt{3} l^2} \sqrt{\frac{E}{\rho}} , \qquad (8)$$

where I is the length of the reed,  $\mu$  is the mass per unit length, and I is the second moment of area of a cross section about the neutral axis of bending (equal to  $bd^3 / 12$ , where b is the breadth of the reed). At the fundamental tone (n = 1) the mode parameter  $\alpha^2$  is 0.8790. The frequencies of the tones increase in the sequence  $(1.194)^2$ ,  $(2.988)^2$ ,  $5^2$ ,  $7^2$ ,  $9^2$ , .... The expressions shown in Eq. (8) neglect the effect of rotary inertia, shear deformation, and the fact that the fixed end of the reed is not free to develop anticlastic curvature. Provided the reed is long compared to both its breadth and thickness, the error associated with neglect of these terms is small and in many cases may be unimportant compared with experimental errors in the determination of reed thickness. As a partial check on Eq. (8), we have measured the frequencies of the first seventeen tones of a flat steel reed prepared from feeler-gage stock for uniformity of thickness and hard-soldered to a massive block for optimal support. The measurements showed small but systematic differences in the sequence of observed and calculated frequencies. Allowing for the fact that E is proportional to  $f_n^2$ , it was concluded that inaccuracies in the theoretical values of  $\alpha_n^2$  should not cause a variation of more than three percent in the value of E as calculated from the frequencies of the various tones. Variations larger than this are not infrequently observed with thin reeds. In some cases, the scatter may be due simply to a lack of uniformity in the thickness of the reed. However, the scatter may also serve as a warning that the cross section of the reed is slightly bowed or warped, an effect which has been observed with splat-cooled reeds [18].

There are two further effects that can lead to errors in the determination of E from  $f_n$ . Both of these effects are most important for the fundamental mode and both are of the sense that causes the apparent modulus to fall below the true value. The first of these is the hydrodynamic, or radiation loading, effect that is shown in Fig. 3(b). The second effect is electromechanical and originates from the presence of the electric field between the specimen and the adjacent electrodes. Because the electrostatic force exerted on the sample varies as the square of the separation distance, the electrostatic coupling is equivalent to a nonlinear spring. The effect on the frequency may be treated by the general procedure described by Den Hartog [19]. For a pair of drive electrodes located at the free end of the reed (the position for which the effect is greatest), the fractional frequency change of  $\Delta f_n/f_n$  associated with a polarizing voltage  $V_p$  is given for small amplitudes of vibration by the expression

$$\Delta f_n / f_n = -C_e V_p^2 / K_n g^2. \tag{9}$$

For the fundamental mode, where the effect is largest, use of a large polarizing voltage (270 V) has been observed to decrease  $f_1^2$  by as much as ten percent. Generally, the voltages used are appreciably smaller than this, and the frequency effect is then greatly reduced. The effect is most likely to be encountered with samples of moderately high damping, where the drive circuit must be used to maintain the vibration amplitude for the frequency-counting interval.

In summary, an accurate absolute determination of Young's modulus by the vibrating reed method requires a uniform flat sample of accurately known thickness, the use of several overtones as a consistency check on uniformity, and careful attention to the experimental conditions.

## • Determination of the strain amplitude

Particularly when dealing with nonlinear effects, it is often desirable to know the strain amplitude at which internal friction measurements are made. From the mode shapes given in the Appendix, it is readily found that the maximum surface strain  $e_{\rm max}$  at the fixed end of the reed is related to the amplitude of motion at the free end,  $A_0$ , by the relation

$$e_{\text{max}} = |2d \alpha_n^2 A_0 / l^2|.$$
 (10)

Use of Eq. (10) for the standard reed used as a thin-film substrate reveals that a strain of 10<sup>-5</sup> is associated with an amplitude  $A_0$  of  $6 \times 10^{-3}$  cm. For successively higher tones, the value of  $A_0$  (for the same strain amplitude) drops rapidly, and is, for example, only  $4 \times 10^{-5}$  cm at the eighth tone. Except for the fundamental mode, the amplitudes used in practice were too small to measure directly with a 50× microscope of sufficient working distance for use outside the vacuum chamber. On the other hand,  $e_{\rm max}$  may be readily calculated by equating the work done per cycle in steady, resonant, forced vibration to the energy dissipated during that cycle. The work done per cycle is  $\pi F_0 A_0$ , where  $F_0$  is the amplitude of the mechanical force exerted by the drive electrodes. The energy dissipated per cycle is  $\delta \cdot K_n A_0^2$ , where  $\delta$  is the logarithmic decrement observed in free decay. We thus obtain

$$A_0 = \pi F_0 / K_n \delta. \tag{11}$$

By evaluation of the quantity  $F_0$  and the use of Eq. (10) we find

$$e_{\text{max}} = \frac{4d}{\pi m l^2} \frac{\alpha_n^2}{f_n^2} \frac{C_e V_p v_1}{g \delta} \times 10^{-5},$$
 (12)

339

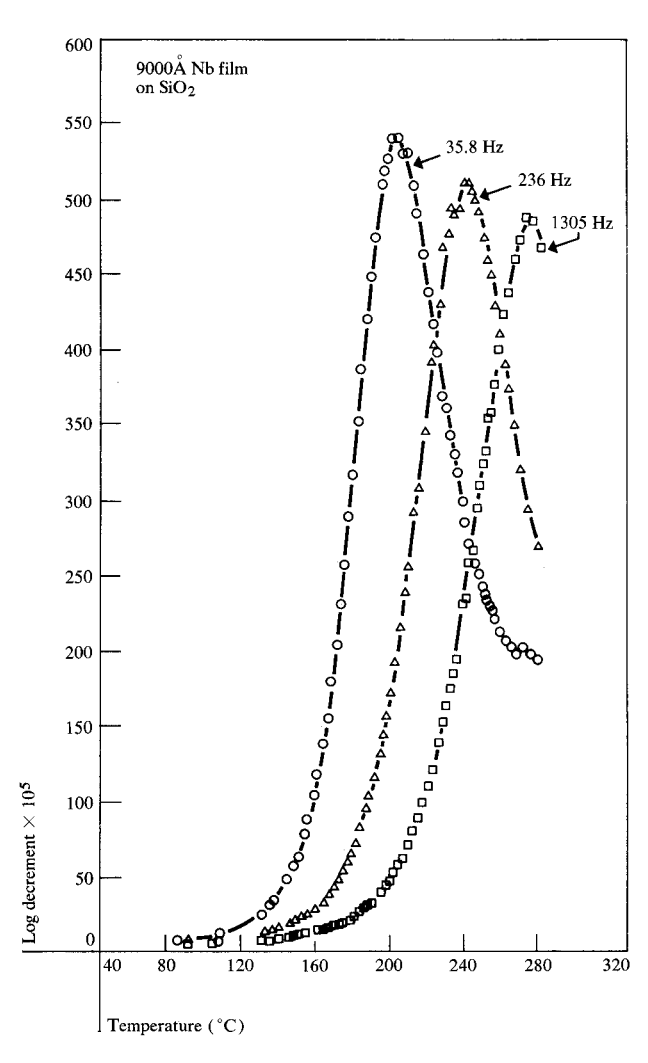


Figure 5 The oxygen Snoek peak in a thin film of niobium, vacuum deposited to a thickness of 0.45- $\mu$ m on each face of a 50- $\mu$ m silica reed. Although the film is only two percent of the thickness of the substrate, note by comparison with Fig. 4 that at the peak the film causes the internal friction of the reed to increase by a factor of more than  $10^3$ .

where  $v_1$  is the amplitude of the ac drive voltage and m is the mass of the sample. The following units have been used: centimeters for d, l, and g; grams for m; picofarads for  $C_e$ , and volts for  $V_p$  and  $v_1$ .

A useful procedure for the determination of  $C_{\rm e}$  is to observe the electromechanical  $\Delta f$ -effect in the fundamental mode and to calculate  $C_{\rm e}$  from Eq. (9). It turns out that most internal friction measurements are made at about the same strain amplitude, regardless of tone, with typical values falling in the range  $e_{\rm max} = 5 \times 10^{-6}$  to  $2 \times 10^{-5}$ . Finally, it may be noted from Eq. (12) that if  $e_{\rm max}$  is held constant, the ac drive voltage  $v_1$  is simply proportional to the internal friction  $\delta$ . This type of relation forms the basis for many electronic feedback systems that have

been designed for the continuous measurement of internal friction at a single frequency [20].

#### • Composite reeds for studies of thin layers

We consider first the damping and frequency of a composite sample produced by deposition of a thin film of thickness t on a reed substrate of thickness d. With the restriction that  $t \ll d$ , Eqs. (13)-(15) apply whether the film is deposited wholly on one side or is shared equally by the two faces of the reed. In practice, the latter arrangement is frequently preferable because it essentially eliminates bending of the reed under the action of the film stress [21]. With the assumptions of an adherent film and a state of simple bending in the reed, the logarithmic decrement  $\delta$  of the composite sample is found to be

$$\delta = \delta_s + (3t/d) (E_t/E_s) \delta_t, \tag{13}$$

where  $\delta_f$  and  $E_f$  represent the logarithmic decrement and Young's modulus of the film, and  $\delta_s$  and  $E_s$  denote the same quantities for the substrate. The factor three in Eq. (13) results from the favorable distribution of strain energy across the section of the reed. It should be noted that Eq. (13) is independent of the distribution of strain along the length of the reed and hence is valid for all tones of vibration. As a reasonable criterion of sensitivity to losses in the film, we may adopt the condition that the second term on the right-hand side of Eq. (13) should be at least equal to the first term,  $\delta_s$ . Hence we obtain the resolution condition

$$\delta_{\rm f} \ge (d/3t) \ (E_{\rm s}/E_{\rm f}) \ \delta_{\rm e},\tag{14}$$

which shows the desirability of using a thin substrate of the lowest possible internal friction. To make practical use of condition (14), we show in Fig. 4 the behavior of a 50-\mum bare silica reed after pedestal mounting and vacuum annealing at 1000°C. (Because of the insulating nature of this sample, the vibration was initiated by tapping the vacuum chamber, and the damping measurements were performed optically. Stroboscopic illumination was used for the frequency measurements.) It is evident from Fig. 4 that the damping of the reed varies smoothly with temperature and is encouragingly small.

Inserting the values  $d = 50 \ \mu \text{m}$  and  $\delta_{\text{s}} = 10^{-5}$  into Eq. (14), and setting  $E_{\text{s}}/E_{\text{f}}$  equal to unity, we find that damping as small as  $2 \times 10^{-3}$  should be detectable in a film only 0.1  $\mu \text{m}$  thick. This measurement sensitivity will permit a broad scope of internal friction studies of thin films

The frequencies  $f_n$  of the composite reed are related to the frequencies  $f_n(0)$  of the bare substrate by the expression

$$\frac{f_n^2}{f_n^2(0)} = 1 + \frac{t}{d} \left( \frac{3E_f}{E_s} - \frac{\rho_f}{\rho_s} \right), \tag{15}$$

where  $\rho_{\rm f}$  and  $\rho_{\rm s}$  are the densities of the film and the substrate, respectively. The two terms of this expression reflect the opposing effects of the elasticity and inertia of the film. The reed frequencies are predicted to increase if  $3E_{\rm f}/E_{\rm s} > \rho_{\rm f}/\rho_{\rm s}$  (as for Al on SiO<sub>2</sub>), and to decrease if  $3E_{\rm f}/E_{\rm s} < \rho_{\rm f}/\rho_{\rm s}$  (as for Au on SiO<sub>2</sub>). Although the magnitude of such a frequency change is large enough to be useful, it generally does not permit an accurate determination of the modulus of a thin film.

The prediction of one interesting frequency effect follows from the data of Fig. 4. Because of the unusual positive value of the temperature coefficient (1/E) dE/dT for fused silica, it can be expected that certain composite reeds may exhibit natural frequencies with remarkably low temperature coefficients  $(1/f_n) df_n/dT$ , a property which may be of some practical interest.

With minor reinterpretation of meaning, Eqs. (13) and (14) apply equally well to the consideration of losses in any thin surface layer, produced for example by ion implantation, electrodeposition, oxide growth, a surface reaction, etc. On the other hand, it may be necessary to replace Eq. (15) with a different expression. For example, if ion implantation produces an altered surface layer of thickness t, modulus  $E_t$  and density  $\rho_t$ , but with conservation of total mass, the appropriate frequency expression becomes [22]

$$\frac{f_n^2}{f_n^2(0)} = 1 + \frac{3t}{d} \left( \frac{E_l}{E_s} - \frac{\rho_l}{\rho_s} \right). \tag{16}$$

#### Illustrative results on thin films

Examples of the use of the apparatus for the study of both splat-cooled amorphous metallic alloys and ion-implantation effects in silicon have been given in earlier publications [8, 18, 22]. We present here two examples of the observation of relaxation phenomena in thin metallic films, using the composite sample approach described in the previous section.

The first example (Fig. 5) shows the excellent resolution of the Snoek peak due to interstitial oxygen in an evaporated film of niobium, as measured at the first, second, and fourth tones of the reed. Measurements of this type provide information on both the concentration of interstitial oxygen and the kinetics of oxygen atom migration in the film. Specifically, from the data of Fig. 5 it can be concluded that the film contains about 0.6 atomic percent of dissolved oxygen, which migrates with an activation energy of 1.17 eV (a value identical with the bulk value). Studies of this type, which will be reported in a later paper, have demonstrated the great susceptibility of niobium films to progressive interstitial contamination during vacuum heat treatments and have given considerable insight into a modification of the normal Snoek

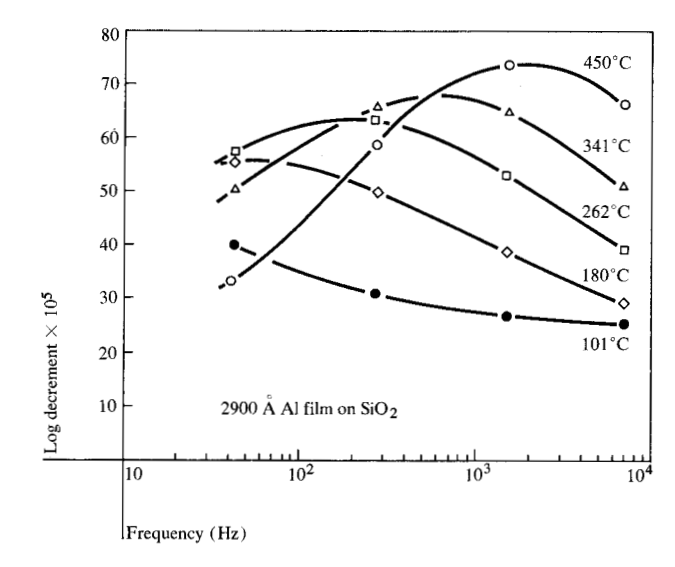


Figure 6 Frequency dependence of the internal friction of an evaporated aluminum film  $(0.29 - \mu \text{m})$  total thickness) deposited equally on both sides of a 50- $\mu \text{m}$  silica reed substrate. Measurements were made at the first, second, third, and eighth tones of vibration, for each temperature indicated.

relaxation behavior which occurs in a thin film subject to a large internal stress.

The second example (Fig. 6) shows a set of measurements taken as a function of frequency on a silica reed supporting a thin aluminum film. These data, which cover a factor of 160 in frequency and include measurements up to the eighth tone, reveal the existence of a relaxation effect which changes in both height and location as the temperature of the sample is changed from 101° to 450°C. The responsible mechanism is as yet unknown. Nonetheless, the results themselves serve as an illustration of the experimental capability provided by the vibrating reed apparatus and emphasize the advantage of a wide frequency range in the characterization of anelastic behavior.

### Concluding remarks

Despite the great increase of interest in thin films and other thin-layer structures that has accompanied the growth of the microelectronics industry, very little work has so far been reported on the characterization of such structures by internal friction measurements [23]. In many situations of practical interest, these measurements can now be made in a convenient and attractive manner with the present apparatus. As for bulk materials, the principal use of the measurements is expected to be the investigation of structural disorder, atomic movements, and defect-related phenomena. However, it is already clear from as yet unreported work that the apparatus can also be useful in other ways. For example, information has been obtained relating to the elastic properties of

341

thin films and the magnetic properties of amorphous alloys. Much further use of the apparatus can be foreseen in the areas of thin films, ion-implantation layers, and splat-cooled materials. In addition, it is likely that other interesting applications may arise in the investigation of electrodeposited thin layers, or layers formed by a surface or interface reaction.

While the apparatus thus has a wide range of possible use, its limitations must not be overlooked. For composite samples, the foremost requirements are that the substrate must be thin, and of a low-damping material which can be supported in a loss-free manner. Despite these limitations, the difficulties associated with the alternative approach of detaching and working with unsupported films would seem to favor adoption of the composite sample approach in most cases. Indeed, rather than regarding the substrate as an enemy to be eliminated or minimized at all costs, the present work illustrates the advantages to be gained from harnessing the substrate as a true working partner of the composite sample. Although the thin layer of interest must dominate the overall dissipation, the substrate can be the means whereby layers of conveniently large area can be examined at the audio frequencies frequently so useful for the investigation of thermally-activated relaxation processes, and over the wide frequency range so important for the characterization of the behavior and the accurate determination of activation energies.

## Appendix: Flexural modes of a cantilever reed

The frequencies of the natural modes are discussed in the section on frequency-related phenomena. The mode shapes of the fundamental and successive odd tones  $(n = 1, 3, 5, \cdots)$  are given by

$$y_n(x) = \frac{A_0}{2} \left\{ \frac{\cosh(2\alpha_n x/l)}{\cosh \alpha_n} + \frac{\sin(2\alpha_n x/l)}{\sin \alpha_n} \right\}. \tag{A1}$$

The shapes of successive even tones  $(n = 2, 4, 6, \cdots)$  are given by

$$y_n(x) = \frac{A_0}{2} \left\{ \frac{\sinh(2\alpha_n x/l)}{\sinh \alpha_n} + \frac{\cos(2\alpha_n x/l)}{\cos \alpha_n} \right\}. \tag{A2}$$

In Eqs. (A1) and (A2),  $y_n(x)$  is the lateral displacement of the reed at a distance x from the center of the reed taken as the origin, and  $A_0$  is the displacement of the free end of the reed (x/l=+0.5). The mode parameters have the values  $\alpha_1=0.29843\pi$ ;  $\alpha_2=0.74709\pi$ ;  $\alpha_3=1.25013\pi$ , and thereafter can be taken simply as  $\alpha_n(n>3)=(n-\frac{1}{2})\pi/2$ . The positions of the nodes may be obtained by solving Eqs. (A1) and (A2) for the condition  $y_n(x)=0$ . Results for the first seven tones are given in Ref. [1], p. 629. The strain energy stored in the reed,  $W_n$ , is obtained by evaluating the integral

$$W_n = \frac{EI}{2} \int_{-1/2}^{+1/2} \left[ y''(x) \right]^2 dx, \tag{A3}$$

where the primes denote differentiation with respect to x. The results for all tones are given by the expression

$$W_n = \frac{1}{2} \left( \frac{4\alpha_n^4 EI}{\beta} \right) A_0^2. \tag{A4}$$

Since the effective spring constant  $K_n$  of each mode is given by the expression

$$W_{n} = \frac{1}{2} K_{n} A_{0}^{2}, \tag{A5}$$

we have

$$K_n = 4\alpha_n^4 EI/l^3. (A6)$$

Combining Eq. (A6) with Eq. (8), we see that

$$f_n = \frac{1}{\pi} \sqrt{\frac{K_n}{m}} \,. \tag{A7}$$

This expression permits a convenient experimental determination of  $K_n$  from the mode frequency  $f_n$  and the mass of the reed, m.

#### **Acknowledgment**

This work was supported in part by the U.S. Army Research Office—Durham. We also acknowledge with thanks many useful comments offered by the referees.

#### References and notes

- 1. A. S. Nowick and B. S. Berry, Anelastic Relaxation in Crystalline Solids, Academic Press, Inc., New York, 1972.
- 2. See, for example, Chapter 20 of Ref. 1.
- 3. P. Duwez, Trans. Am. Soc. Metals 60, 607 (1967).
- H. S. Chen and C. E. Miller, Rev. Sci. Instr. 41, 1237 (1970).
- 5. W. Benoit, Helv. Phys. Acta 37, 205 (1964).
- G. P. Weiss and D. O. Smith, Rev. Sci. Instr. 34, 522 (1963).
- V. S. Postnikov, V. K. Belonogov, and I. V. Zolutuhkin, Fiz. Metal. i. Metalloved. 23, 946 (1967), translated in Sov. Phys. – Met. Metallog. 23, 173 (1967).
- S. I. Tan, B. S. Berry, and W. F. J. Frank, Ion Implantation in Semiconductors and Other Materials, ed. B. L. Crowder, Plenum Press, Inc., New York, 1973, p. 19.
- R. A. Tomboulian, Research Report RC 396, IBM Thomas J. Watson Research Center, Yorktown Heights, New York, 1961.
- 10. A. D. N. Smith, J. Sci. Instr. 28, 106 (1951).
- 11. Ref. 1, p. 18.
- 12. I. Langmuir, J. Am. Chem. Soc. 35, 107 (1913).
- J. Yarwood, High Vacuum Techniques, John Wiley & Sons, Inc., New York, 1956, p. 102.
- 14. J. P. Hobson, J. Vac. Sci. Technol. 7, 557 (1970).
- See, for example, Handbook of Thin Film Technology, eds. L. I. Maissel and R. Glang, McGraw-Hill Book Co., Inc., New York, 1970, pp. 1-25.
- W. W. Scott and R. K. MacCrone, Rev. Sci. Instr. 39, 821 (1968).
- 17. Ref. 1, p. 500.
- B. S. Berry and W. C. Pritchet, J. Appl. Phys. 44, 3122 (1973).

- J. P. Den Hartog, Mechanical Vibrations, third edition, McGraw-Hill Book Co., Inc., New York, 1947, p. 427.
- 20. For collected references, see Ref. 1, pp. 587 and 592.
- E. Klokholm and B. S. Berry, J. Electrochem. Soc. 115, 823 (1968).
- S. I. Tan, B. S. Berry, and B. L. Crowder, Appl. Phys. Lett. 20, 88 (1972).
- 23. In addition to the references given earlier on vibrating reed apparatus, some work has also appeared on high-frequency (5 MHz) ultrasonic attenuation measurements on self-supporting gold films, e.g., K. Uozumi, T. Nakada, and A. Kinbara, Thin Solid Films 12, 67 (1972). Attenuation measurements may also be possible on attached films by the propagation of a high-frequency surface wave; see G. W.

Farnell and E. L. Adler, *Physical Acoustics IX*, edited by W. P. Mason and R. N. Thurston, Academic Press, Inc., New York, 1972, p. 35. Although high frequency techniques can be useful for the investigation of dislocation and various electronic effects, low frequency techniques are generally better suited to the study of thermally activated atomistic processes.

Received May 13, 1974

The authors are located at the IBM Thomas J. Watson Research Center, Yorktown Heights, New York 10598.